Sunflower-like fluorescent Self-assembledmorphologiesformed byPyridothiazole based Aggregation Induced Emission (AIE)dye and its cell imaging applications

VivekshinhKshtriya[a],Bharti Koshti[a], Ashadul Haque[b], AnkitGangrade[b], Ramesh Singh, Khashti Ballabh Joshi,[c] Sujoy Bandyopadhyay,[a] Dhiraj Bhatia,[b]* Nidhi Gour[a] *

[a] Department of Chemistry, Indrashil University, Kadi, Mehsana, Gujarat, India;E-mail: nidhigour@gmail.com

[b] Biological Engineering Discipline, Indian Institute of Technology Gandhinagar, Palaj, 382355, Gandhinagar, India E-mail:dhiraj.bhatia@iitgn.ac.in

[c] Department of Chemistry, Dr. Hari Singh Gour, Sagar University, Madhya Pradesh, India

Abstract:

We report for the very first-time self-assembly of 4-(5-methoxythiazolo[4,5-b]pyridin-2-yl)-N,N-dimethylaniline **(TPA)** to fluorescent sunflower-like architectures**.** Interestingly, **TPA** exhibits blue fluorescence in visible light at 385 nm and the fluorescence is not affected by photo-induced quenching rather the fluorescence keeps on increasing with time under broad day light. The morphologies of self-assembled structures of **TPA** were studied at various concentrations in dimethyl sulphoxide (DMSO) and Tetrahydrofuran (THF). The microscopic studies through SEM and fluorescence microscopy reveal the formation of sunflower-like

fluorescent self-assemblies. Further, our study revealed that the sunflower shaped assemblies formed by **TPA** exhibitfluorescence under blue, green, and red channels that can be evinced by the fluorescence spectroscopy and microscopy. Hence **TPA** exhibits panchromatic emission properties and it reveals tunable emission properties under different excitation wavelengths. Further, AIE properties of **TPA** were evinced by recording fluorescence in THF under varying concentrations of water and doing solvent chromic studies.Finally,the utility of **TPA** as a cell imaging agent was studied in human breast cancer cell lines (MDA-MB-231) which suggested **TPA** can penetrate the cell membrane and can be effectively used as a cell labeling dye.

Introduction:

Self-assembly is a very important bottom-up approach for the design of novel micro or nano architectures with diverse applications in science and technology .[1] The structure formation through self-assembly is mediated at a supramolecular level through non-covalent forces like hydrogen bonding,[2-4] vander Waals forces,[5] electrostatic interactions,[6, 7] pi-pi stacking [8-10] and hydrophobic forces of attraction to name a few,[11, 12] These non-covalent forces mediate the formation of nano-architectureslike fibril,[10, 13, 14] nano-flower,[15, 16] nano-tape,[17] rods,[18, 19] etc.which have immense applications in diverse research fields such as chemistry,[20]life science,[21]material science,[22] and nanotechnology[10, 23],owing to their utility for the design ofnovel catalysts,[24, 25] optoelectronics[26], solar cell,[27]and biomaterials[28-30]which is very important for the development of new materials and processes.

Aggregation-induced emission is also a very important photophysical phenomenonwhich is governed by the restricted rotation of molecules. The restricted rotation causes twisted intermolecular charge transfer (TICT) state which changes to locally excited state during aggregation process.[31, 32].In2001 Tang et al. for the very first time reported 1-methyl-1, 2, 3, 4, 5-pentaphenylsiloleAIE molecule,[32]which later revealedwide range of applicationsin different

fieldssuch as tissue engineering,[33] celltracing,[34], OLED,[35] bioprobes[36], etc. The advantage of AIE dye over the conventional dye is they remain unaffected by quenching and their fluorescence keep on increasing as aggregation increases unlike conventional dyes which need to be protected from light and the fluorescence is quenched with time and aggregation.

Our group has been interested in assessing the self-assembling properties of amino acids,[4, 37] peptide,[38-43] oligonucleotide,[38] biopolymers and heterocyclic compounds.[44, 45]Recently, we also reported self-assembly of pyridothiazole-based, aggregation-induced emission-enhancement (AIEE) luminogen 4-(5-methoxy-thiazolo[4,5-*b*]pyridin-2-yl)benzoic acid (**PTC1**) and its application for the sensitive detection and monitoring of amyloid fibrillation.[45] Hence, motivated from our previous studies we designed a new pyridothiazole scaffold which is more similar to another molecular rotor Thioflavin T and do not have a donor acceptor pair.to assess its utility as an AIE dye. Hence newpyridothiazole based conjugate 4-(5-methoxythiazolo[4,5-b]pyridin-2-yl)-N,N-dimethylaniline **(TPA)**was synthesized and its aggregation properties were studied. Herein, this manuscript we report for the very first time sunflower-like self-assembled architectures formed by TPA and its aggregation induced emission properties and applications in cell imaging (Figure 1)**.**Nakanishi et al. reported the first flower-like structure for C-60 fullerene.[16, 46]Thereafter, some other groups also reported flower-like self-assembled structures for different molecules[47-49]A very recent literature also report formation of well-defined nano-sunflowersby the self-assembly of rod coil amphiphilic molecules.[49]However, there is no report wherein formation of fluorescent flower like assemblies are reported. Moreover, there is rarely a report wherein formation of well-defined self-assembly by AIE luminogens is illustrated. Hence the studies reported in the manuscript are very novel and of immense utility for design and fabrication of novel nanoarchitectures.

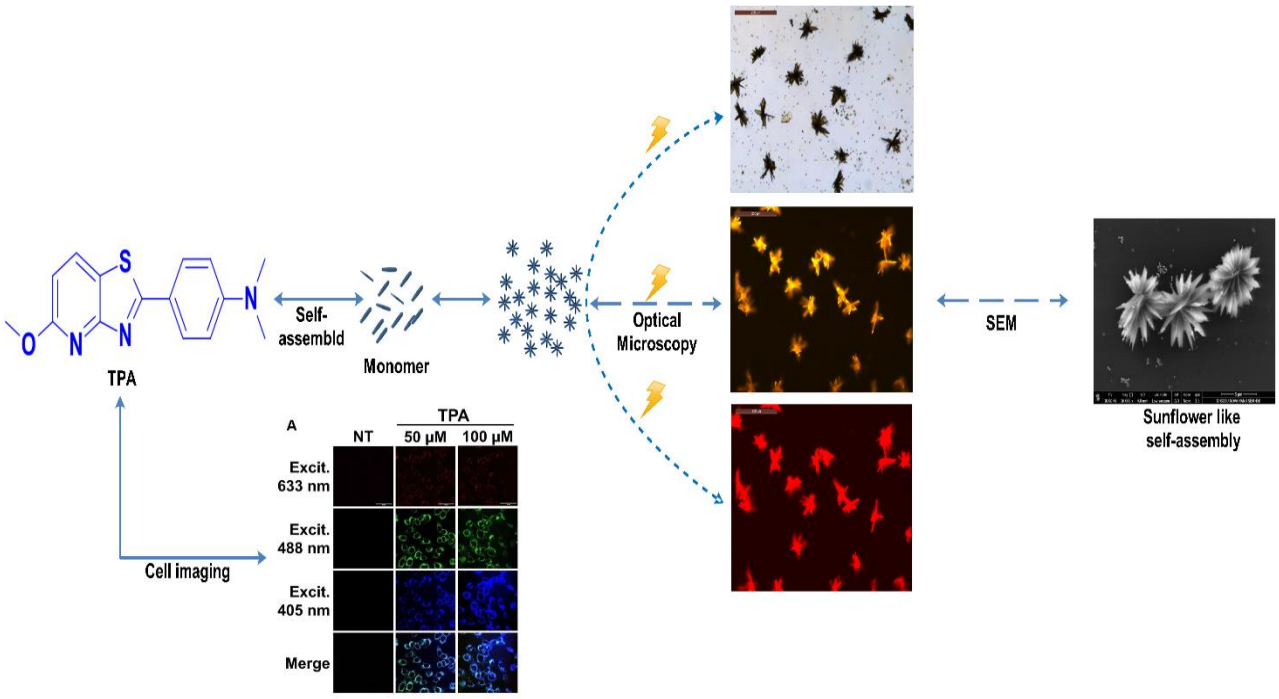

Figure 1. Graphical representation of self-assembled structuresformed by **TPA** and its application in cell imaging.

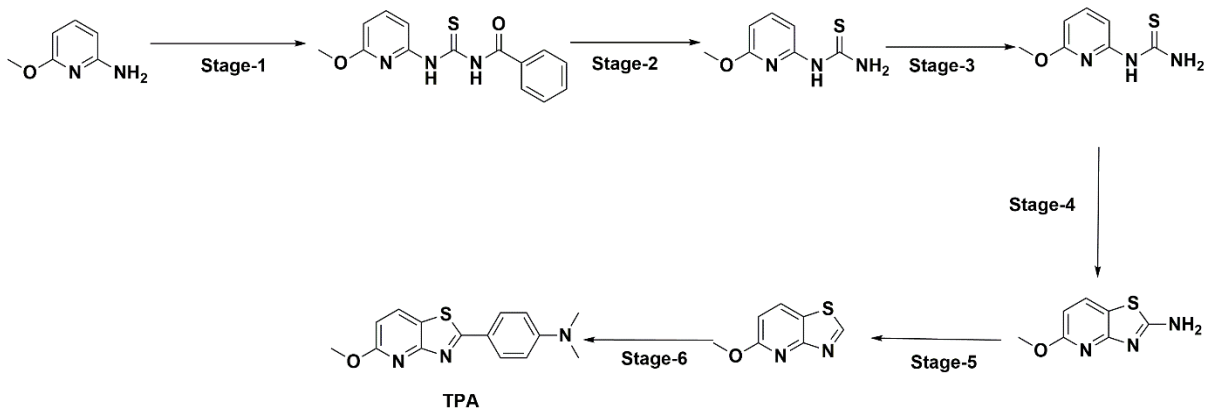

Scheme 1. Scheme for the synthesis of **TPA.**

4-(5-methoxythiazolo[4,5-b]pyridin-2-yl)-N,N-dimethylaniline (**TPA**) construct was synthesized by using the standard synthetic methodologies in 6 steps starting from 2-amino-6-methoxy pyridine via Scheme 1. To introduce a thiazole moiety, first, the amino group of

2-amino-6-methoxy pyridine was coupled with the benzoyl isothiocyanate followed by the hydrolysis leading to the formation of a thiourea derivative of 6-methoxy pyridine. Next intramolecular cyclization was carried out in the presence of lithium bromide and bromine by using acetic acid as a solvent to yield a fused thiazole ring. In the next step, deamination was carried out, which is necessary for further C−C coupling. Further, C−H activation was done by using palladium acetate and Xantphos, and C−C coupling was done with 4-bromo-N,N-dimethylaniline, which upon subsequent hydrolysis yielded**TPA.** The as-synthesized **TPA** was characterized by ^{1}H and ^{13}C NMR spectroscopy and its purity ascertained through analytical HPLC. After complete structural characterization, the self-assembling properties of **TPA** were studied in solution to know the structure formation and to understand its morphology at the supramolecular level. The self-assembly properties of **TPA** molecules were studied at various concentrations from 1 to 10 mM in Water, THF, and DMSO. Notably,**TPA** show the flower-like self-assembled structure in DMSO and THF only. Figure 2 illustrated sunflower like self-assembled structures formed by **TPA**in SEM. The SEM image of TPA (1mM) at higher magnification reveals beautiful sunflower like morphology. Since the size of assemblies were big, they could also be observed under optical and fluorescence microscope and the flowers appear yellow green and red under green and red filter respectively. Intense yellow green fluorescence observed in green channel may be attributed to high fluorescence intensity (Figure 3, Figure 4). As we increased the concentration of TPA, there was no change in flower-like morphologies in DMSO as well as THF however more aggregation could be seen as concentration increases from 2-10mM.

Interestingly, when we added water, sunflower like structures revealed a morphological transition to tape likestructures. Figure 5 reveal tape like aggregates of **TPA**at 1 mM concentration. Herein too, as we increased the concentration of there was no morphological

change howeverthe thickness of the tape-like structure is increased at higher concentrations from 2 to 10 mM.

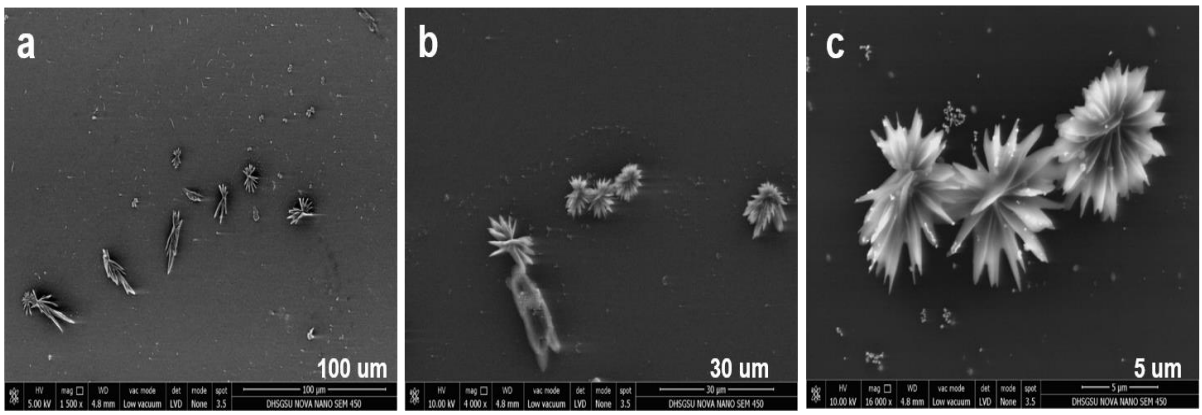

Figure 2. SEM images of **TPA**in DMSOunder different magnifications**a)** 100 µM,b) 30 µM, c) 5 µM.

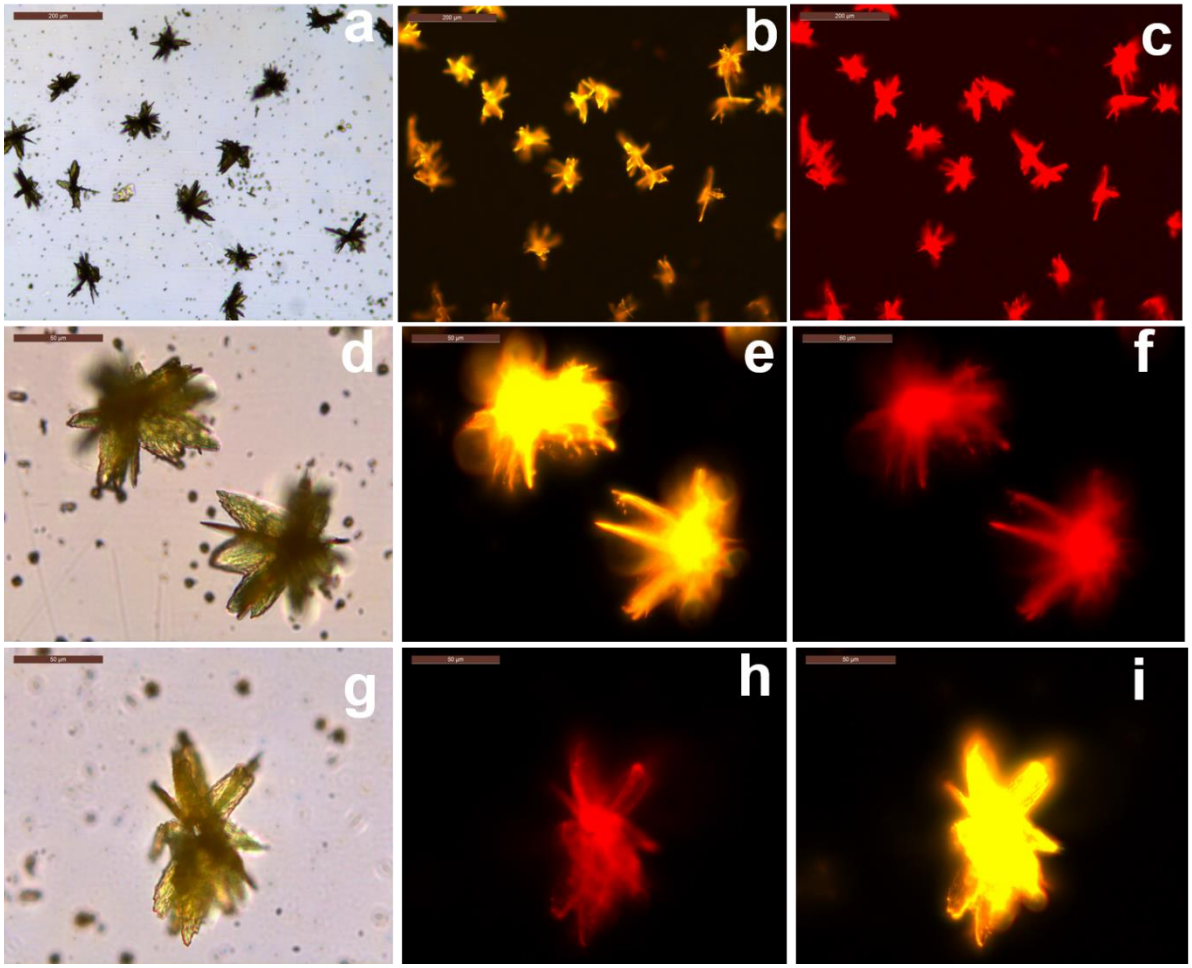

Figure 3. Microscopic images of **TPA** under bright field, green filter and red filter in DMSO

a-c) at 8 mM concentration under 20X, scale bar 200 µm; d-f) at 8 mM concentration under 40X, scale bar 50µm; g-i) at 9 mM concentration under 40X, scale bar 50µm

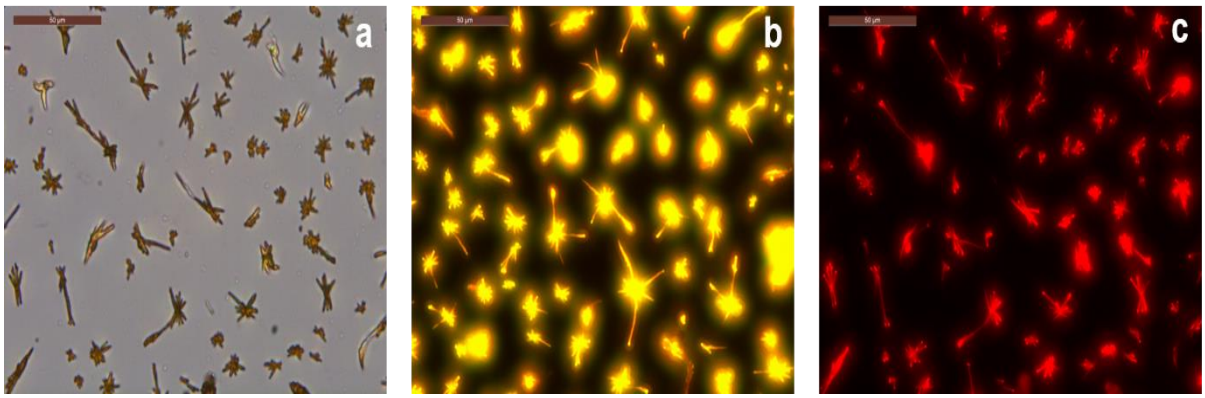

Figure 4. Optical and fluorescence microscopic images of **TPA in** THF. (a) in bright field (b) under green filter,(c) under red filter at 1 mM concentrationunder40X, scale bar 50 µm.

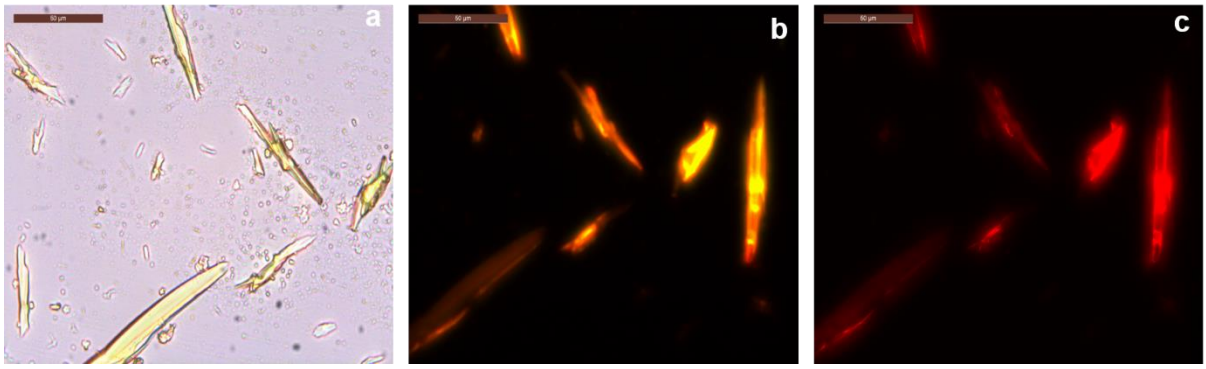

Figure 5. Optical microscopy images of TPA in water at 1 mM concentration.

The aggregation-induced emission properties of **TPA** were assessed by recording fluorescence of TPA in mixture of THF: water from 0 to 100 %. The study revealed that in the neat THF, **TPA** molecules shows a lower fluorescent intensity (Figure 6) . In contrast, when we increased the water fraction due to increased aggregation the fluorescence isregularly increased till 60 % fraction of water in THF. As the water concentration if increased further, the fluorescence intensity if lowered due to decreases aggregation as the amphiphilicity of solventis reduced from 70-90% water in THF.The microscopic

investigations too reveal maximal aggregation in 60% water in THF while less aggregation in THF and water alone.

Figure 6. The vial images of TPA with increasing % of water in THF a) 0% b)10 % c) 20 % d)30 % e) 40 % f) 50 % g)60 % h) 70 % i) 80 % j)90 % k)100 % Water.

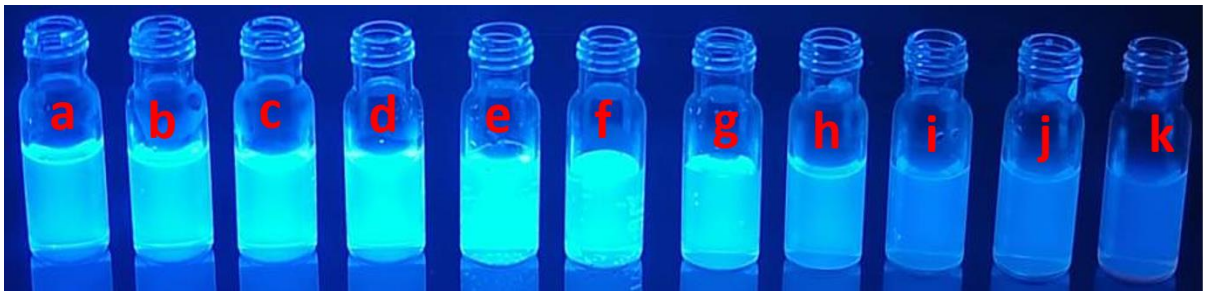

Figure 7. Increasing % of water in DMSO a) 0% b)10 % c) 20 % d)30 % e) 40 % f) 50 % g)60 % h) 70 % i) 80 % j)90 % k)100 % Water

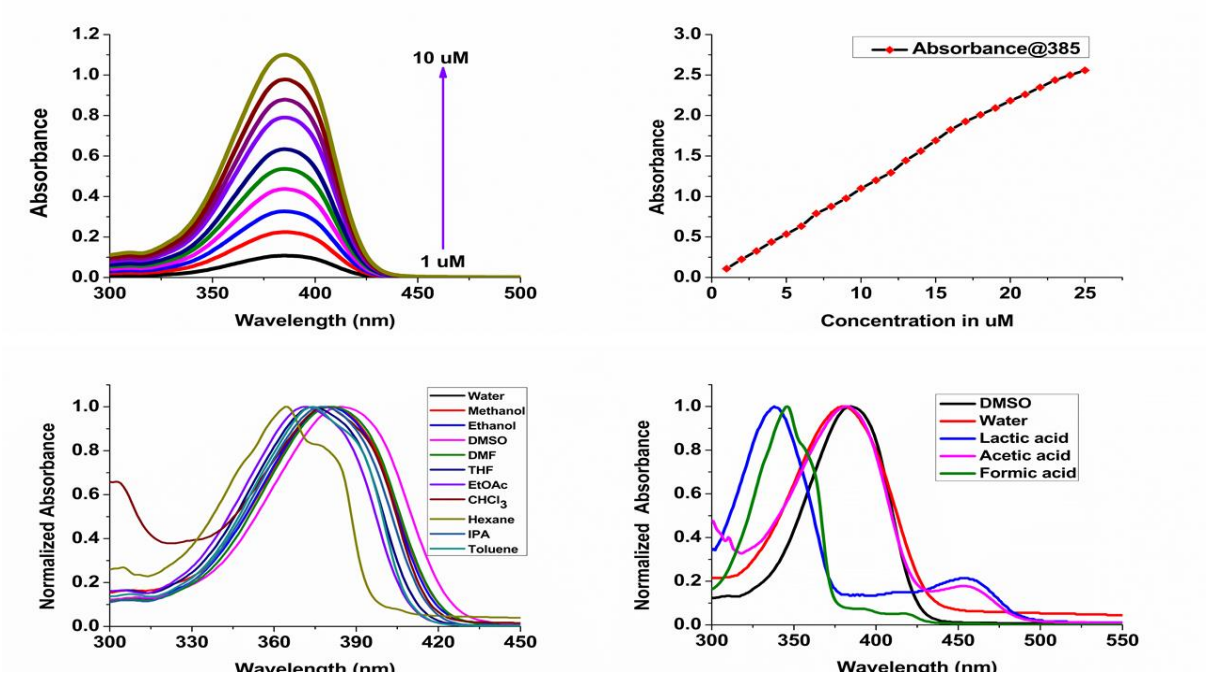

Figure 8. UV-visible spectra of **TPA** a) UV-visible spectra of TPA at 1 to 10 µM concentration, b) straight-line graph between 1 to 25 µM concentration at 385 nm, c) Normalized UV-Vis spectra of **TPA** in the different solvent at 10µM concentration, d) UV-visible spectra in different organic acid.

To understand the photophysical properties of **TPA** in more detail, UV-Visible spectra of TPA was recorded from1 to 10 µM concentration**.TPA** itselfshow blue color fluorescence in solution in broad daylight and reveal absorbancemaximaat 385 nm. It may be also noted the Lambert beer's law is obeyedand the straight-line graph showing linear relationship between absorbance and concentration could be observed to 1 to 25 µM.Further, we performed the solvent dependent study of **TPA** in different solvents having varying polarities such as water, methanol, ethanol, DMSO, DMF, THF, EtOAc, $CHCl_3$, Hexane, and IPA.The solvatochromic studies revealed that as the polarity of solvent increased the absorbance spectra of**TPA**reveal bathochromic shift or redshift.The maximum bathochromic shift has been observed in case of DMSO while maximum hypsochromic shift or blue shift could be observed in n-Hexane. Further, we also recorded the UV-visible spectra of **TPA** in weak acid such as acetic acid, lactic acid, and formic acid.Surprisingly,UV visible spectra in formic acid

and lactic acid reveal hypsochromic shift with the new peaks appearing in the region of 425-475 nm. This study suggest TPA might also reveal sensitivity to pH and may be used as proton sensor, the studies of which need to be done in greater details in future.

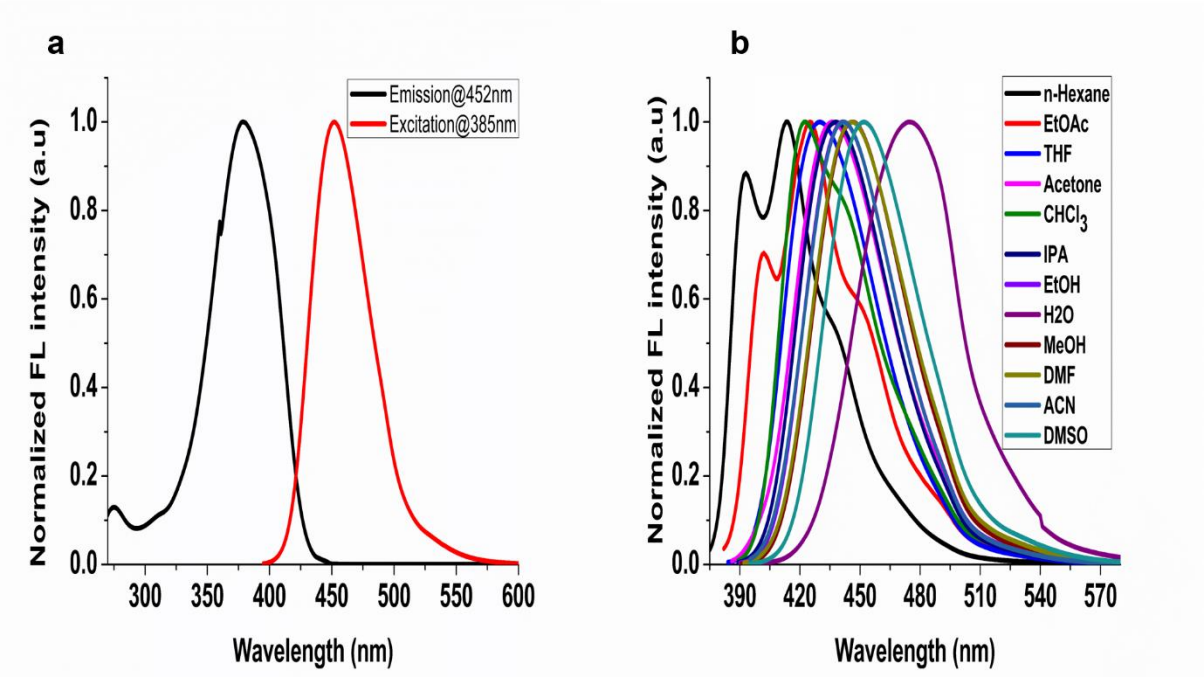

Figure 9. Fluorescence spectra of **TPA**a) Normalized graph of **TPA**at emission@452 and excitation@385 nm b) Normalized fluorescence graphof **TPA**in different solvent

Further, we also recorded the fluorescence spectra of **TPA**andfound its emission maxima at 465 nm at 10 µM concentration in DMSO.

TPA showed strong cyan colour fluorescence in tetrahydrofuran (THF) organic solvent with a peak at 452 nm (Figure 9a). Emission spectra depict a considerable red shift as the solvent polarity increases; emission maximum shifts from 410 nm in n-Hexane to 478 nm in water (Figure 9b). Such positive solvatochromism in emission indicates a highly polar excited state, presumably originating from the donor-acceptor 4-(5-methoxythiazolo[4,5-b]pyridin-2-yl)-N,N-dimethyl aniline moiety.

Finally the utility of TPA for cell imaging applications were assessed by incubating TPA with fixed human The **TPA**-treated cells were excited with three lasers, and corresponding emission was collected as follows. (excitation 633 nm; emission 643 to 796 nm, excitation 488 nm; emission 500 to 600 nm, excitation 405 nm; emission 415 to 500 nm).

Approximately 30 cells were selected from three different images, and their fluorescence intensity was quantified (Figure 10).

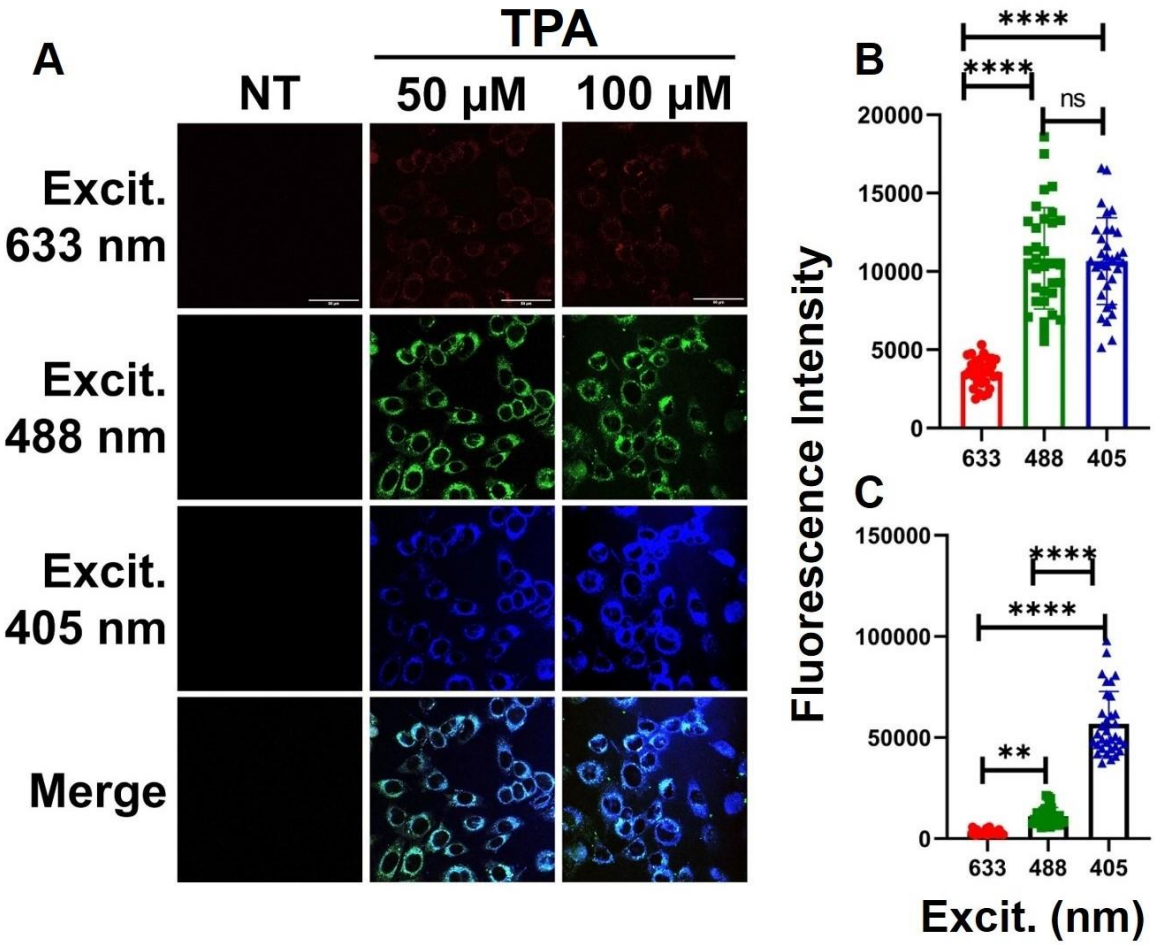

Figure 10. Representative **(A)** confocal microscopy images of human breast cancer cell line (MDA-MB-231) treated with 50 µM and 100µM synthesized **TPA** compound. Fluorescence quantification of **(B)**50 µM and **(C)**100uM concentration**TPA** treated cells wereplottedat all three excitation wavelengths. **** Indicates significance level at $P < 0.0001$, * indicates significance level at $P < 0.0329$, and ns indicates no significance between the fluorescence intensities.

Materials and method:

Self-assembling properties of TPA

The self-assembly property of **TPA** were assessed by scanning electron microscopy and optical microscopy, at 1 to 10 mM concentration.

Scanning electron microscopy (FE-SEM)

SEM images were taken using a JSM7600F (Jeol) FE-SEM 450 microscope (the accelerating voltage ranging from 1 to 15 kV). SEM samples were prepared on silicon wafers. A 10 μL**TPA** of a 1mM solution were dispensed and dried at room temperature. The samples were analyzed without gold coating under a low vacuum.

Atomic Force Microscopy (AFM)

Neat and co-incubated solutions of **TPA** were imaged under an atomic force microscope. The samples were placed on freshly cleaved muscovite mica surfaces followed by imaging with an AFM (INNOVA, ICON analytical equipment, Bruker, operating under the acoustic AC mode (AAC or tapping mode), with the aid of a cantilever (NSC 12(c) from MikroMasch, Silicon Nitride Tip) by NanoDrive version 8 software. The force constant was 2.0 N/m, while the resonant frequency was ~276 kHz. All of the images were taken in the air at rt, with the scan speed of 1.5 lines/sec. The data analysis was done using the nanoscope analysis software. The sample-loaded substrates were dried at dust-free space under a 40W lamp for 30 min followed by high-vacuum drying and subsequently examined under AFM.

Preparation of stock solution:

All the microscopic and spectroscopic studiesof **TPA**were done using10 mM stock solution of **TPA** in DMSO.

UV visible study

The UV-visible spectra havebeen recorded at 1 to 25 μMconcentration by using the 10 mM stock solution of **TPA**in different solvents.The spectra were recorded by usingShimadzu UV-1900 UV-vis spectrophotometer.

Fluorimetric analysis

The excitation and emission spectra of **TPA** were recorded at 10 μM concentration in DMSO. The emission spectra of **TPA** were recorded by giving an excitation wavelength as 385 nm and recorded from 395 to 800 nm. Similarly, the excitation spectra were recorded from 200 to 800 nm, where the maximum emission wavelength (λem) was found to be 452 nm. The experiment has been performed on Jasco spectrofluorometer FP 8300.

Solvent dependent study of TPA

The solvent dependent study has been done at 10 μM concentration by using 10 mM stock solution in DMSOthrough UV-visible and Spectrofluorometer instrument in DMSO, THF, Water,Hexane, Etoc, IPA, chloroform, ACN, MeOH, Ethanol, Acetone, acetic acid, formic acid, lactic acid.

Cytotoxic assay:

Cell imaging:

Human breast cancer (MDA-MB-231) cells were grown in DMEM cell culture media supplemented with 10% FBS and 1% antibiotic in a 5% CO2 incubator. First, the cells were seeded onto a glass coverslip and fixed with 4% paraformaldehyde. Later the fixed cells were treated with 50 μM and 100 mM TPA for 15 min at room temperature. The coverslips were then mounted on a glass slide, and images were captured in Leica confocal microscope.

Conclusions.

In conclusion, we have reported a new pyridothiazole basedaggregation induced emission luminogen4-(5-methoxythiazolo[4,5-b]pyridin-2-yl)-N,N-dimethylaniline **(TPA) and its** self-assembly to well-defined sunflower like morphologies in DMSO and THF. These structures were analysed extensively by SEM, optical microscopy and fluorescence microscopy. As the concentration of water was increased there was gradual morphological transition from

sunflower to tape like structures.The aggregation induced emission properties of TPA were studied extensively by solvatochromic studies. Finally, the utility of TPA as a cell imaging agentwas studied in human breast cancer cell lines (MDA-MB-231) which suggested **TPA** can be effectively used as cell labelling dye and the cells revealed panchromatic emission and fluorescence under blue green and red channels albeit with different fluorescence intensities.

Reference:

1. Paulson, J. A.; Mesbah, A.; Zhu, X.; Molaro, M. C.; Braatz, R. D., Control of self-assembly in micro-and nano-scale systems. *Journal of Process Control* **2015,***27*, 38-49.
2. Corradi, E.; Meille, S. V.; Messina, M. T.; Metrangolo, P.; Resnati, G., Halogen bonding versus hydrogen bonding in driving self-assembly processes. *Angewandte Chemie International Edition* **2000,***39* (10), 1782-1786.
3. Paramonov, S. E.; Jun, H.-W.; Hartgerink, J. D., Self-assembly of peptide− amphiphile nanofibers: the roles of hydrogen bonding and amphiphilic packing. *Journal of the American Chemical Society* **2006,***128* (22), 7291-7298.
4. Gour, N.; Kanth P, C.; Koshti, B.; Kshtriya, V.; Shah, D.; Patel, S.; Agrawal-Rajput, R.; Pandey, M. K., Amyloid-like structures formed by single amino acid self-assemblies of cysteine and methionine. *ACS chemical neuroscience* **2018,***10* (3), 1230-1239.
5. Nerngchamnong, N.; Yuan, L.; Qi, D.-C.; Li, J.; Thompson, D.; Nijhuis, C. A., The role of van der Waals forces in the performance of molecular diodes. *Nature nanotechnology* **2013,***8* (2), 113-118.
6. Reches, M.; Gazit, E., Self-assembly of peptide nanotubes and amyloid-like structures by charged-termini-capped diphenylalanine peptide analogues. *Israel journal of chemistry* **2005,***45* (3), 363-371.
7. Yan, Y.; Huang, J.; Tang, B. Z., Kinetic trapping–a strategy for directing the self-assembly of unique functional nanostructures. *Chemical Communications* **2016,***52* (80), 11870-11884.
8. Gazit, E., A possible role for π-stacking in the self-assembly of amyloid fibrils. *The FASEB Journal* **2002,***16* (1), 77-83.
9. Reches, M.; Gazit, E., Casting metal nanowires within discrete self-assembled peptide nanotubes. *Science* **2003,***300* (5619), 625-627.
10. Gazit, E., Self-assembled peptide nanostructures: the design of molecular building blocks and their technological utilization. *Chemical Society Reviews* **2007,***36* (8), 1263-1269.
11. Sánchez-Iglesias, A.; Grzelczak, M.; Altantzis, T.; Goris, B.; Perez-Juste, J.; Bals, S.; Van Tendeloo, G.; Donaldson Jr, S. H.; Chmelka, B. F.; Israelachvili, J. N., Hydrophobic interactions modulate self-assembly of nanoparticles. *ACS nano* **2012,***6* (12), 11059-11065.
12. Jiang, L.; Cao, S.; Cheung, P. P.-H.; Zheng, X.; Leung, C. W. T.; Peng, Q.; Shuai, Z.; Tang, B. Z.; Yao, S.; Huang, X., Real-time monitoring of hydrophobic aggregation reveals a critical role of cooperativity in hydrophobic effect. *Nature communications* **2017,***8* (1), 1-8.
13. Gazit, E., Self assembly of short aromatic peptides into amyloid fibrils and related nanostructures. *Prion* **2007,***1* (1), 32-35.
14. Reches, M.; Porat, Y.; Gazit, E., Amyloid fibril formation by pentapeptide and tetrapeptide fragments of human calcitonin. *Journal of Biological Chemistry* **2002,***277* (38), 35475-35480.

15. Zhou, S.; Wang, L.; Chen, M.; Liu, B.; Sun, X.; Cai, M.; Li, H., Superstructures with diverse morphologies and highly ordered fullerene C 60 arrays from 1: 1 and 2: 1 adamantane–C 60 hybrid molecules. *Nanoscale* **2017,***9* (42), 16375-16385.
16. Nakanishi, T.; Ariga, K.; Michinobu, T.; Yoshida, K.; Takahashi, H.; Teranishi, T.; Moehwald, H.; G. Kurth, D., Flower-shaped supramolecular assemblies: hierarchical organization of a fullerene bearing long aliphatic chains. *Small* **2007,***3* (12), 2019-2023.
17. Murai, K.; Inagaki, K.; Hiraoka, C.; Minoshima, S.; Kinoshita, T.; Nagata, K.; Higuchi, M., Mineralization of magnetic nano-tape in self-organized nanospace composed of nucleopeptides and peptides. *CrystEngComm* **2019,***21* (23), 3557-3567.
18. Li, L.-s.; Walda, J.; Manna, L.; Alivisatos, A. P., Semiconductor nanorod liquid crystals. *Nano Letters* **2002,***2* (6), 557-560.
19. Huynh, W. U.; Dittmer, J. J.; Alivisatos, A. P., Hybrid nanorod-polymer solar cells. *science* **2002,***295* (5564), 2425-2427.
20. Dujardin, E.; Mann, S., Bio-inspired materials chemistry. *Advanced Materials* **2002,***14* (11), 775-788.
21. Xu, X.; Jian, Y.; Li, Y.; Zhang, X.; Tu, Z.; Gu, Z., Bio-inspired supramolecular hybrid dendrimers self-assembled from low-generation peptide dendrons for highly efficient gene delivery and biological tracking. *ACS nano* **2014,***8* (9), 9255-9264.
22. Dickinson, E.; Leser, M. E., *Food colloids: self-assembly and material science*. Royal Society of chemistry: 2007.
23. Reches, M.; Gazit, E., Molecular self-assembly of peptide nanostructures: mechanism of association and potential uses. *Current Nanoscience* **2006,***2* (2), 105-111.
24. Guler, M. O.; Stupp, S. I., A self-assembled nanofiber catalyst for ester hydrolysis. *Journal of the American Chemical Society* **2007,***129* (40), 12082-12083.
25. Yamada, Y. M.; Sarkar, S. M.; Uozumi, Y., Amphiphilic self-assembled polymeric copper catalyst to parts per million levels: click chemistry. *Journal of the American Chemical Society* **2012,***134* (22), 9285-9290.
26. Li, H.; Choi, J.; Nakanishi, T., Optoelectronic functional materials based on alkylated-π molecules: self-assembled architectures and nonassembled liquids. *Langmuir* **2013,***29* (18), 5394-5406.
27. Cui, K.; Chiba, T.; Omiya, S.; Thurakitseree, T.; Zhao, P.; Fujii, S.; Kataura, H.; Einarsson, E.; Chiashi, S.; Maruyama, S., Self-assembled microhoneycomb network of single-walled carbon nanotubes for solar cells. *The Journal of Physical Chemistry Letters* **2013,***4* (15), 2571-2576.
28. Orbach, R.; Mironi-Harpaz, I.; Adler-Abramovich, L.; Mossou, E.; Mitchell, E. P.; Forsyth, V. T.; Gazit, E.; Seliktar, D., The rheological and structural properties of Fmoc-peptide-based hydrogels: the effect of aromatic molecular architecture on self-assembly and physical characteristics. *Langmuir* **2012,***28* (4), 2015-2022.
29. Orbach, R.; Adler-Abramovich, L.; Zigerson, S.; Mironi-Harpaz, I.; Seliktar, D.; Gazit, E., Self-assembled Fmoc-peptides as a platform for the formation of nanostructures and hydrogels. *Biomacromolecules* **2009,***10* (9), 2646-2651.
30. Mahler, A.; Reches, M.; Rechter, M.; Cohen, S.; Gazit, E., Rigid, self-assembled hydrogel composed of a modified aromatic dipeptide. *Advanced Materials* **2006,***18* (11), 1365-1370.
31. Li, J.; Qian, Y.; Xie, L.; Yi, Y.; Li, W.; Huang, W., From Dark TICT State to Emissive quasi-TICT State: The AIE Mechanism of N-(3-(benzo [d] oxazol-2-yl) phenyl)-4-tert-butylbenzamide. *The Journal of Physical Chemistry C* **2015,***119* (4), 2133-2141.
32. Luo, J.; Xie, Z.; Lam, J. W.; Cheng, L.; Chen, H.; Qiu, C.; Kwok, H. S.; Zhan, X.; Liu, Y.; Zhu, D., Aggregation-induced emission of 1-methyl-1, 2, 3, 4, 5-pentaphenylsilole. *Chemical communications* **2001,** (18), 1740-1741.
33. Liu, H.; Xiong, L. H.; Kwok, R. T. K.; He, X.; Lam, J. W. Y.; Tang, B. Z., AIE bioconjugates for biomedical applications. *Advanced Optical Materials* **2020,***8* (14), 2000162.

34. Li, K.; Zhu, Z.; Cai, P.; Liu, R.; Tomczak, N.; Ding, D.; Liu, J.; Qin, W.; Zhao, Z.; Hu, Y., Organic dots with aggregation-induced emission (AIE dots) characteristics for dual-color cell tracing. *Chemistry of Materials* **2013,***25* (21), 4181-4187.
35. Shi, H.; Xin, D.; Gu, X.; Zhang, P.; Peng, H.; Chen, S.; Lin, G.; Zhao, Z.; Tang, B. Z., The synthesis of novel AIE emitters with the triphenylethene-carbazole skeleton and para-/meta-substituted arylboron groups and their application in efficient non-doped OLEDs. *Journal of Materials Chemistry C* **2016,***4* (6), 1228-1237.
36. Ding, D.; Li, K.; Liu, B.; Tang, B. Z., Bioprobes based on AIE fluorogens. *Accounts of chemical research* **2013,***46* (11), 2441-2453.
37. Koshti, B.; Singh, R.; Kshtriya, V.; Walia, S.; Bhatia, D.; Gour, N., Amyloid like aggregates formed by the self-assembly of proline and Hydroxyproline. **2021**.
38. Gour, N.; Kedracki, D.; Safir, I.; Ngo, K. X.; Vebert-Nardin, C., Self-assembling DNA–peptide hybrids: morphological consequences of oligonucleotide grafting to a pathogenic amyloid fibrils forming dipeptide. *Chemical Communications* **2012,***48* (44), 5440-5442.
39. Gour, N.; Verma, S., Bending of peptide nanotubes by focused electron and ion beams. *Soft Matter* **2009,***5* (9), 1789-1791.
40. Gour, N.; Barman, A. K.; Verma, S., Controlling morphology of peptide-based soft structures by covalent modifications. *Journal of Peptide Science* **2012,***18* (6), 405-412.
41. Abraham, J. N.; Gour, N.; Bolisetty, S.; Mezzenga, R.; Nardin, C., Controlled aggregation of peptide–DNA hybrids into amyloid-like fibrils. *European Polymer Journal* **2015,***65*, 268-275.
42. Gour, N.; Mondal, S.; Verma, S., Synthesis and self-assembly of a neoglycopeptide: morphological studies and ultrasound-mediated DNA encapsulation. *Journal of Peptide Science* **2011,***17* (2), 148-153.
43. Barman, A. K.; Gour, N.; Verma, S., Morphological transition triggered by mannose conjugation to a cyclic hexapeptide. *ARKIVOC* **2013,***2*, 82-99.
44. Gour, N.; Kshtriya, V.; Koshti, B.; Gangrade, A.; Haque, A.; Bhatia, D., Synthesis and Characterization of the Fluorescent Self-Assembled Structures Formed by Benzothiazolone Conjugates and Applications in Cellular Imaging. **2021**.
45. Gour, N.; Kshtriya, V.; Gupta, S.; Koshti, B.; Singh, R.; Patel, D.; Joshi, K. B., Synthesis and Aggregation Studies of a Pyridothiazole-Based AIEE Probe and Its Application in Sensing Amyloid Fibrillation. *ACS Applied Bio Materials* **2019,***2* (10), 4442-4455.
46. Nakanishi, T.; Michinobu, T.; Yoshida, K.; Shirahata, N.; Ariga, K.; Moehwald, H.; Kurth, D. G., Nanocarbon superhydrophobic surfaces created from fullerene-based hierarchical supramolecular assemblies. *Advanced Materials* **2008,***20* (3), 443-446.
47. Wagalgave, S. M.; Padghan, S. D.; Al Kobaisi, M.; La, D. D.; Bhamidipati, K.; Puvvada, N.; Bhosale, R. S.; Bhosale, S. V.; Bhosale, S. V., Selectivity and bio-compatibility of self-assembled chiral flower-like and helical nanostructures. *New Journal of Chemistry* **2020,***44* (41), 18092-18101.
48. Chen, L.-Y.; Zhang, Z.-D.; Wang, W.-Z., Self-assembled porous 3D flowerlike β-In2S3 structures: synthesis, characterization, and optical properties. *The Journal of Physical Chemistry C* **2008,***112* (11), 4117-4123.
49. Zhou, Y.; Yao, Y.; Xue, M., Well-defined nano-sunflowers formed by self-assembly of a rod-coil amphiphile in water and their morphology transformation based on a water-soluble pillar [5] arene. *Chemical Communications* **2014,***50* (59), 8040-8042.